Nuclear Instruments and Methods in Physics Research A 608 (2009) 86–91

Contents lists available at ScienceDirect

Nuclear Instruments and Methods in Physics Research A

journal homepage: www.elsevier.com/locate/nima

# GEMGrid: a wafer post-processed GEM-like radiation detector

V.M. Blanco Carballo [a,*], Y. Bilevych [b], M. Chefdeville [b], M. Fransen [b], H. van der Graaf [b], C. Salm [a], J. Schmitz [a], J. Timmermans [b]

[a] University of Twente/Mesa+ Institute for Nanotechnology, Hogekamp 3214, PO Box 217, 7500 AE Enschede, The Netherlands
[b] Nikhef, Science Park 105, 1098 XG Amsterdam, The Netherlands

ARTICLE INFO

*Article history:*
Received 18 May 2009
Received in revised form
5 June 2009
Accepted 8 June 2009
Available online 18 June 2009

*Keywords:*
GEM
Micromegas
SU-8
CMOS post-processing
Above-IC
Microsystems
Radiation detectors
Proportional chambers

ABSTRACT

This paper presents a new wafer post-processed micropatterned gaseous radiation detector called GEMGrid. The device consists of a GEM-like structure fabricated with SU-8 photoresist directly on top of a Timepix chip with zero gap distance. The detector characteristics have been studied in several gas mixtures. The device is capable of tracking minimum ionizing particles and exhibits good energy resolution on $^{55}$Fe decays. We further show a strongly improved mechanical robustness of these GEM-like structures as compared to a pillar-supported integrated Micromegas.



## 1. Introduction

The possibility of combining a GEM or Micromegas foil with a pixelized readout chip for radiation imaging has been proven in the past few years [1–4]. This kind of detector allows for the replacement of the wires, anode pads and readout electronics of conventional gaseous radiation imaging detectors. To avoid misalignment between holes in the grid and pixels in the readout chip and inactive pixel areas, microelectronics fabrication techniques can be used to manufacture a Micromegas directly on a microchip (InGrid). Recently we have shown the results [5] of such a grid integrated on top of Timepix [6], as well as Medipix2 [7] pixel readout chips.

Inspired on the Micro-Bulk Micromegas detector [8], we present in this paper the first results of a GEM-like structure, integrated on top of a Timepix chip using wafer post-processing techniques. This structure combines the mechanical robustness of a GEM with the manufacturing advantages of microtechnology (including inherently good alignment between GEM holes and readout pads). Cylindrical holes can be produced to prevent charging-up [9], and the hole diameter of the metal layer hole and the insulator can be chosen independently with a high degree of freedom and precision.

In this paper we report the response of such detectors to charged particles and $^{55}$Fe radiation in He/i$C_4H_{10}$ and Ar/i$C_4H_{10}$ gas mixtures. Also, tests are reported to evidence the superior mechanical robustness of this new approach.

## 2. Detector fabrication

The GEMGrid fabrication process follows the same scheme as InGrid fabrication [5]. The only difference is in the mask used to define where the supporting dielectric material will remain. A schematic of the process flow is shown in Fig. 1. It consists of the following steps:

(1) Deposition by spin coating of a SU-8 negative photoresist layer on top of a CMOS chip or wafer. The layer thickness can be chosen freely in the range 1–1000 μm.
(2) UV exposure of the photoresist through a mask aligned with the pixels of the chip. Exposed regions will crosslink and become the grid-supporting structure while unexposed parts will be dissolved in a final step.
(3) Deposition of a 1-μm-thick aluminum layer by sputtering on top of the SU-8 layer and posterior patterning by wet etching of this electrode to produce 30 μm diameter holes. The patterning is done such that the grid holes are aligned with the pixels of the chip.

* Corresponding author. Tel.: +31 53 489 2729; fax: +31 53 489 1034.
*E-mail address:* v.m.blancocarballo@utwente.nl (V.M. Blanco Carballo).

0168-9002/$ - see front matter © 2009 Elsevier B.V. All rights reserved.
doi:10.1016/j.nima.2009.06.023

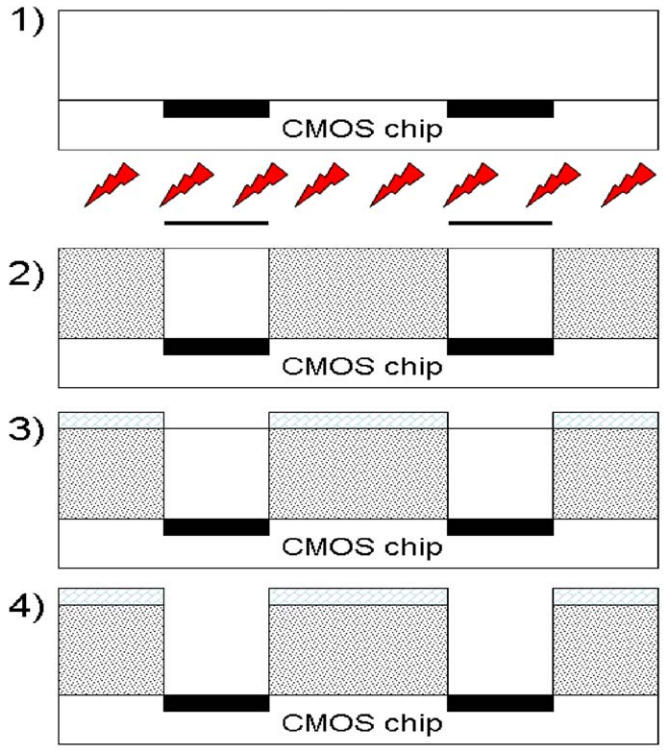


**Fig. 1.** GEMGrid fabrication process flow.

(4) Development of the unexposed SU-8 to release the final structure.

More details can be found in [5] and references therein.

Prior to the fabrication of the GEMGrid structure the chips were covered with a spark protection layer [10].

The use of microelectronic techniques in the fabrication process assures very good dimensional precision combined with high-materials purity, an advantage in relation to ageing [11]. This approach leads to submicrometer alignment precision between the GEM-like structure and the readout chip, and to gap variations no larger than a few percent. The dimensions of the structure can be adapted to fit the geometry of many striped or pixelized readout chips. The fabrication process is done at low temperature; mild plasmas and low stress are involved. Consequently, in the three prototypes tested all the chips remained functional after the fabrication of the GEMGrid structure. A SEM image of the device is shown in Fig. 2.

## 3. Experimental set-up

For device testing, the chip was wire bonded onto a printed circuit board and mounted into a small chamber in which a 3-cm-drift gap field cage is used to ensure good field uniformity. This same field cage works as cover of the chamber and seals the region around the chip. Feedthroughs made in the field cage allow flushing the gas into the chamber. In some experiments a 10-cm-drift gap field cage was also used in the chamber.

A picture of an assembled Timepix/Ingrid chamber is shown in Fig. 3.

The Timepix chip [6] contains 65536 pixels arranged in an area of about $14\,\text{mm} \times 14\,\text{mm}$. It has three detection modes: it provides, either the number of electron avalanches recorded at a pixel during a preset acquisition time window (Medipix mode), the arrival time of an avalanche (Timepix mode) or the time over

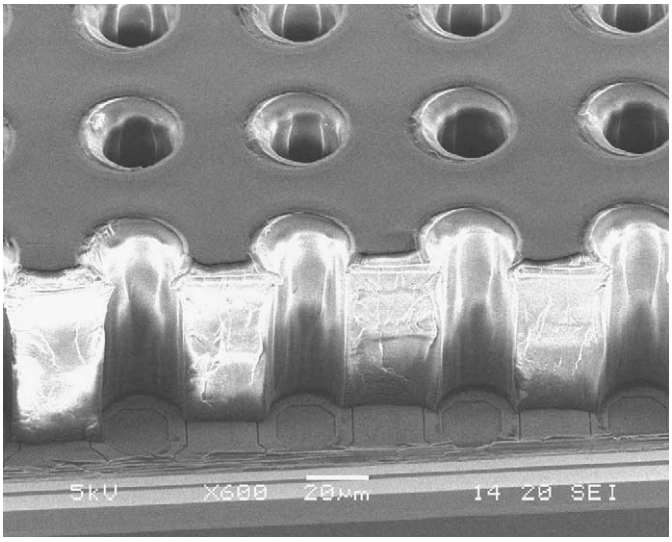


**Fig. 2.** SEM image of the detector, fabricated with 55 µm thick SU-8. The holes in the insulator (SU-8) are 30 µm in diameter, and slightly wider in the metal (aluminum) because of overetching.

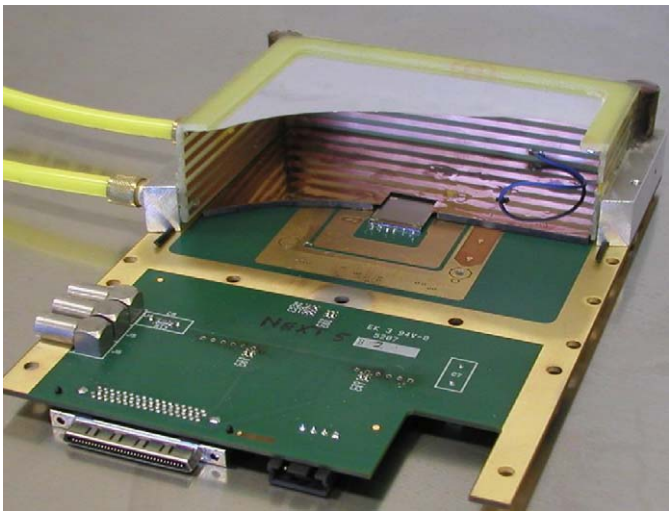

**Fig. 3.** Cut view of an assembled Timepix/InGrid chamber. The chip in the centre, wire bonded to the PCB can be seen through a cross-section of the field cage.

threshold of the input signal (TOT mode). To be detectable, the charge induced by an avalanche at a pixel input should be higher than the pixel threshold, set around 800 electrons.

The output of the printed circuit board was connected through a MUROS2 [12] interface to a computer, to read out the output signals of the chip. Pixelman [13] software provides the interface to control and read the chip.

## 4. Results

For the first measurement the chamber was flushed with Helium/$iC_4H_{10}$ (77/23) and high voltage was applied to the GEM electrode. (While suitable for initial tests, isobutane may be less attractive in permanent setups where ageing is a concern [11].) The detector was irradiated with an $^{55}$Fe source. At −420 V on the grid, electron clouds from $^{55}$Fe conversions in the gas could be clearly seen in the pixel matrix. Fig. 4 shows some $^{55}$Fe clouds,

where the black pixels correspond to electron avalanches detected at the pixels of the chip.

During irradiation with the $^{55}$Fe several naturally occurring α-particle tracks were detected,see Fig. 5. Although the single-electron efficiency was not high, tracks of electrons emitted by $^{90}$Sr were visible in He/i$C_4H_{10}$ (70/30) when −470 V was applied to the grid electrode, see Fig. 6. Using the Timepix chip in Timepix mode, such tracks can be reconstructed in 3D, as shown in Fig. 7.

As we use exactly the same dimensions and materials for Micromegas and GEM structures, the two can be directly compared in many respects. Here we report on their high-voltage capability. In several gas mixtures, we measured the onset voltage of sparking. With prototypes constructed as shown in Fig. 2, the spark voltage is significantly lower for the GEM-like structure. This is summarized in Table 1. Since the electric field configuration is similar in both cases, the integrated GEM-like

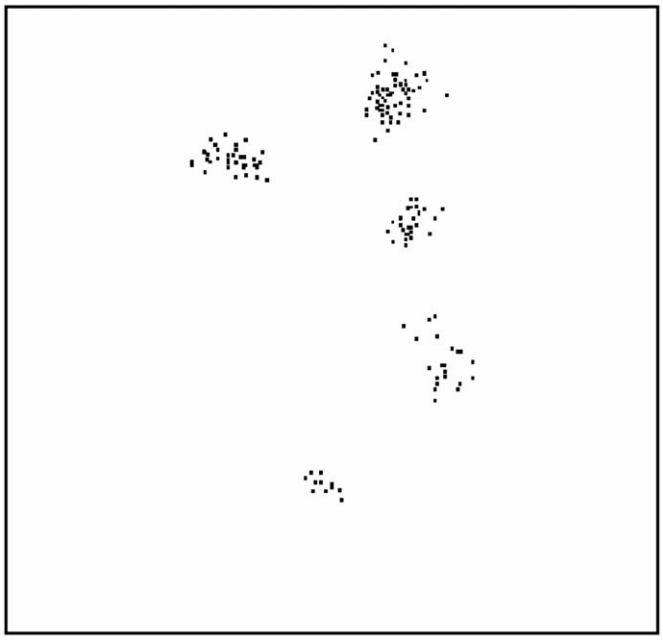

**Fig. 4.** Image of five $^{55}$Fe clouds in He/i$C_4H_{10}$ (77/23) spread over the chip area recorded with a 10 cm drift gap chamber.

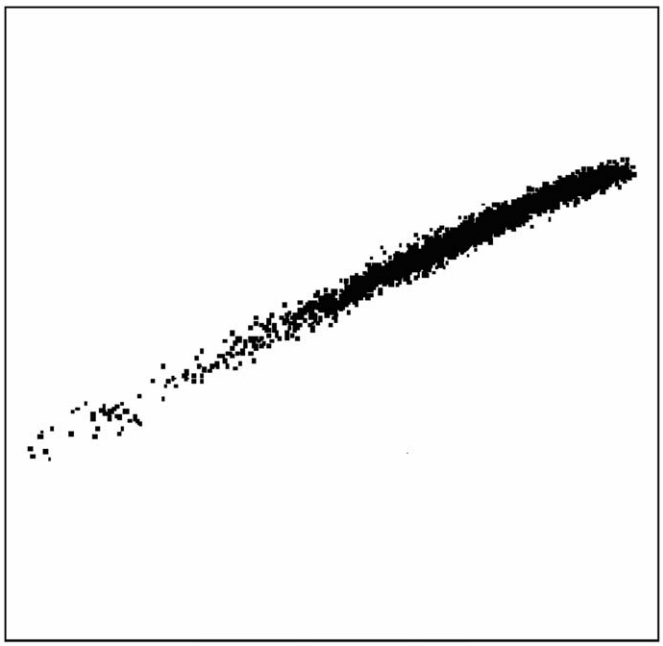

**Fig. 5.** An alpha particle crossing the detector area.

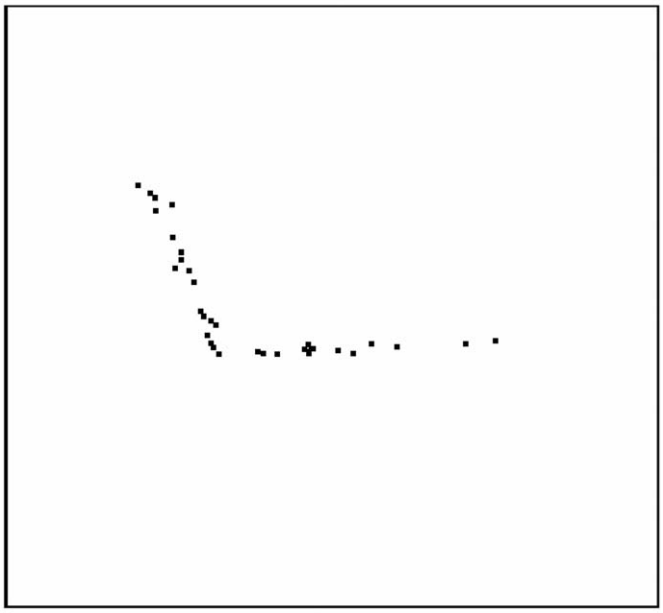

**Fig. 6.** Two tracks of electrons emitted by a $^{90}$Sr source crossing the detector area.

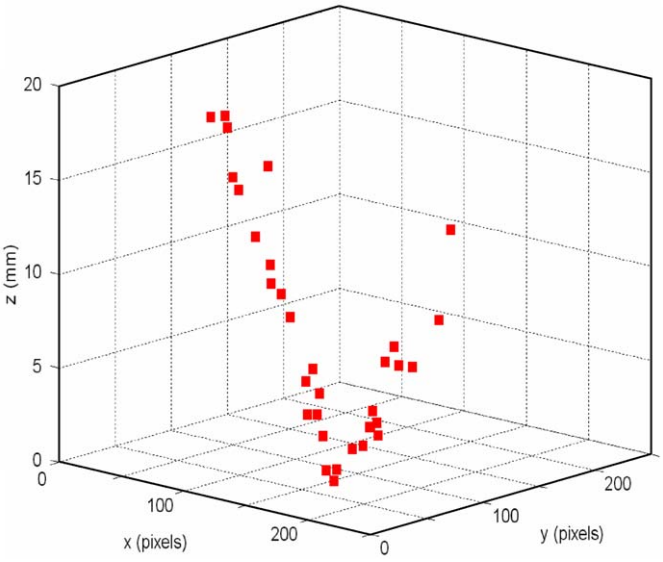


**Fig. 7.** 3D reconstructed image of the two tracks shown in Fig. 6.

**Table 1**
Spark limit for GEMGrid and InGrid detectors.

| | GEMGrid (V) | InGrid (V) |
|---|---|---|
| He/Iso (77/23) | −420 | −470 |
| Ar/Iso (95/5) | −280 | −360 |
| Ar/Iso (80/20) | −380 | −470 |
| Ar/$CO_2$ (70/30) | −315 | −480 |

structure reaches significantly lower maximum gain than the integrated Micromegas-like structure.

The difference was assumed to be a direct result of the recessed aluminum: the aluminum holes have a larger diameter than the holes in the SU-8, see Fig. 2. The SU-8 surface may charge up, yielding to a higher spark probability. This problem is not present in Micromegas-like structures. The Micromegas pillars are always well hidden under the metal electrode.

To verify whether the diameter mismatch between the metal and the SU-8 is the root cause of the lower voltage breakdown value in the GEM-like structure, a modified device was built. It is also fabricated following the process flow shown in Fig. 1 but with recessed SU-8. The SEM image of this device is shown in Fig. 8. In this case the holes in the insulator are 46 μm in diameter while the holes in the metal are 30 μm in diameter. In Ar/$iC_4H_{10}$ (95/5), we have established that this redesigned GEM-like structure maintains −350 V before sparking, therefore closing in on the Micromegas performance.

Using a 10-cm-drift gap field cage the electron transverse diffusion in Ar/$iC_4H_{10}$ (95/5) is sufficient to spread the primary charge of an $^{55}$Fe conversion across the chip surface. The number of activated pixels is then proportional to the number of primary electrons. (It would equal the number of primary electrons if the single electron efficiency were 100% and if no two drifting electrons would create an avalanche at the same pixel.) Summing up the number of hit pixels in every $^{55}$Fe cloud the spectrum can be reconstructed, as shown in Fig. 9. A good energy resolution of 12.4% FWHM is obtained.

Counting the number of activated pixels is better done in the escape peak, as it contains half the number of electrons of the main peak, leading to a lower probability of two electron avalanches in the same pixel. Counting the number of detected electrons in the escape peak and assuming 110 primary electrons, the variation of the single-electron efficiency with the grid voltage could be measured, as presented in Fig. 10. A single electron efficiency of 82% is reached at −350 V on the grid.

The gas gain of the modified GEMGrid device was measured using a He/$iC_4H_{10}$ (77/23) gas mixture. The device was irradiated with a collimated $^{55}$Fe source. The maximum pulse height at the grid was measured. To deduce the gain from the maximum pulse height it was assumed that an $^{55}$Fe event produces 160 primary electrons on average in this gas mixture. The results are shown in Fig. 11. Stable operation at gains exceeding $10^4$ has been achieved,

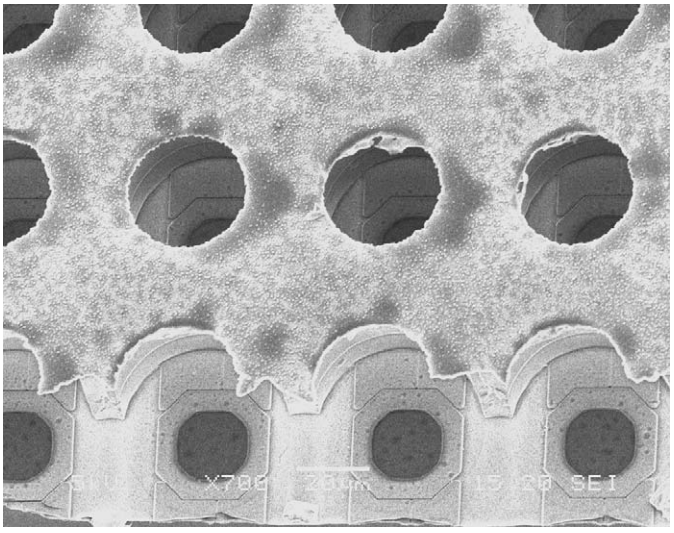

**Fig. 8.** SEM image of the GEMGrid modified version with recessed insulator walls. The insulator hole diameter is 46 μm, while the metal holes are 30 μm in diameter.

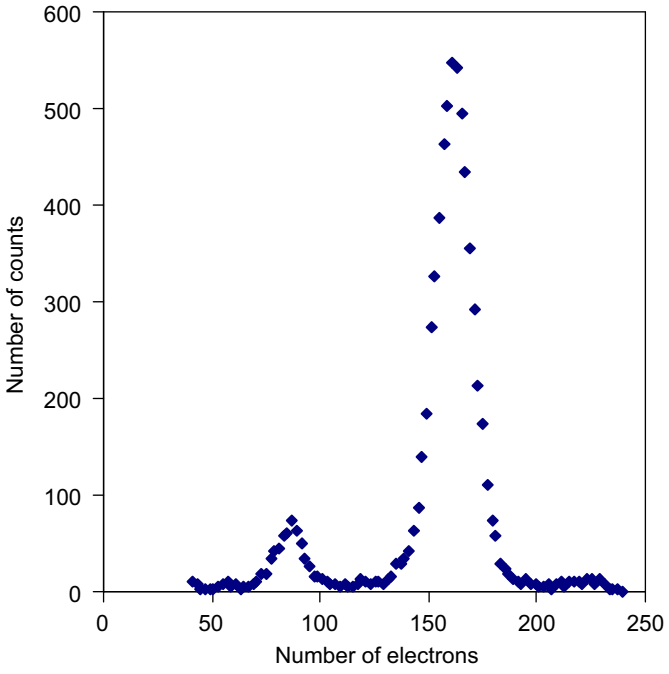


**Fig. 9.** Detector performance illustrated from X-ray radiation response, operating at -340 V on the grid in Ar/$iC_4H_{10}$ (95/5). The histogram shows a count spectrum of $^{55}$Fe radioactive decays reconstructed from counting single electron avalanches. Assuming 220 electrons as the number of primary electrons in the main peak from an $^{55}$Fe conversion a single electron efficiency of 73% is deduced.

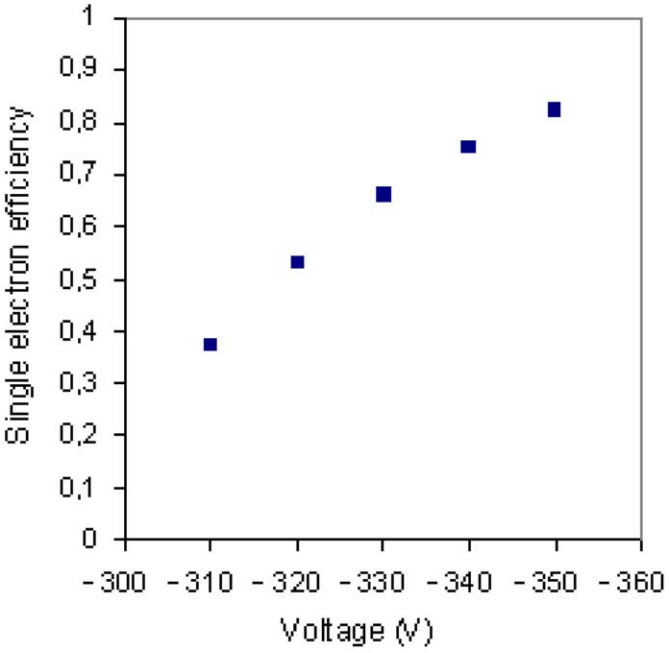


**Fig. 10.** Single electron efficiency as a function of the grid voltage deduced from the number of electrons in the escape peak of the $^{55}$Fe spectrum.

indicating that the detector can reach an even higher single-electron efficiency than quantified above. Assuming exponential charge distribution and a pixel threshold of 1000 electrons a single-electron efficiency of more than 90% is expected at −420 V [14].

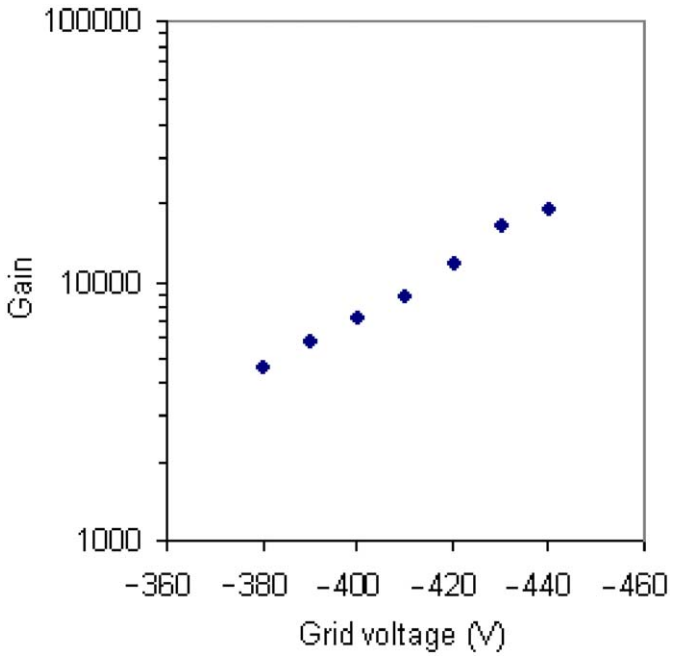


**Fig. 11.** Measured gas gain vs. grid voltage for He/$iC_4H_{10}$ (77/23).

## 5. Structural strength of InGrid and GEMGrid

To compare the mechanical robustness of Micromegas-like and GEM-like structures, several devices were built on dummy silicon wafers and subjected to mechanical and air-flow attacks.

First we investigated the ruggedness of the detectors when an object impacts on the detector. This test was inspired by the ball-drop tests used in the liquid crystal display community [15] and the ballpoint pen drop test known from fingerprint sensors [16]. Our first test consists in dropping a ballpoint pen from a certain distance above the device to assess the damage.

For the InGrid device, as seen in Fig. 12, just dropping the ballpoint pen from a 1 cm distance can cause severe damage as the pen can scratch the grid after bouncing. As conducting as well as insulating material is detached from the detector surface, this damage can be assumed to make the device malfunction. For the GEMGrid the damage is less pronounced as the pen bounces on the device and does not scratch the grid. Instead, only an imprint of the tip of the ballpoint pen is observed on the GEMGrid, as shown in Fig. 13. All material seems to remain in place, even when a higher drop distance of 5 cm is employed.

Comparing Figs. 12 and 13, the GEMGrid detector exhibits much better robustness against vertical mechanical attacks. Still, even in the GEMGrid case a ballpoint drop will adversely affect the detector functionality locally around the impact point.

The drop ballpen test caused serious damage to the InGrid. To investigate the behavior under weaker forces, the tip of a Dektak profilometer from Veeco [17] was moved along the grid of both InGrid and GEMGrid. The maximum force that can be applied by the profilometer was 15 mg and no damage was observed for any device. In the InGrid case a mechanical displacement of the grid can be observed but it is restored to its original position once the force stops.

In our previous works [18,19] we have shown reliability issues of InGrid detectors that arise after moisture exposure. It was found that supporting SU-8 pillars can delaminate from the substrate under humid conditions. The same works report that a larger delamination force is required for larger-area SU-8 features.

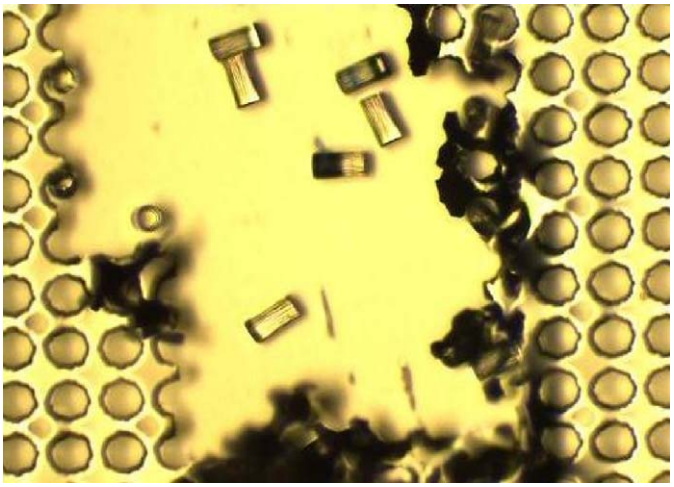

**Fig. 12.** Optical microscope image of an InGrid after the drop test from 1 cm height. A large scratch in the grid is produced and pillars are detached from the substrate.

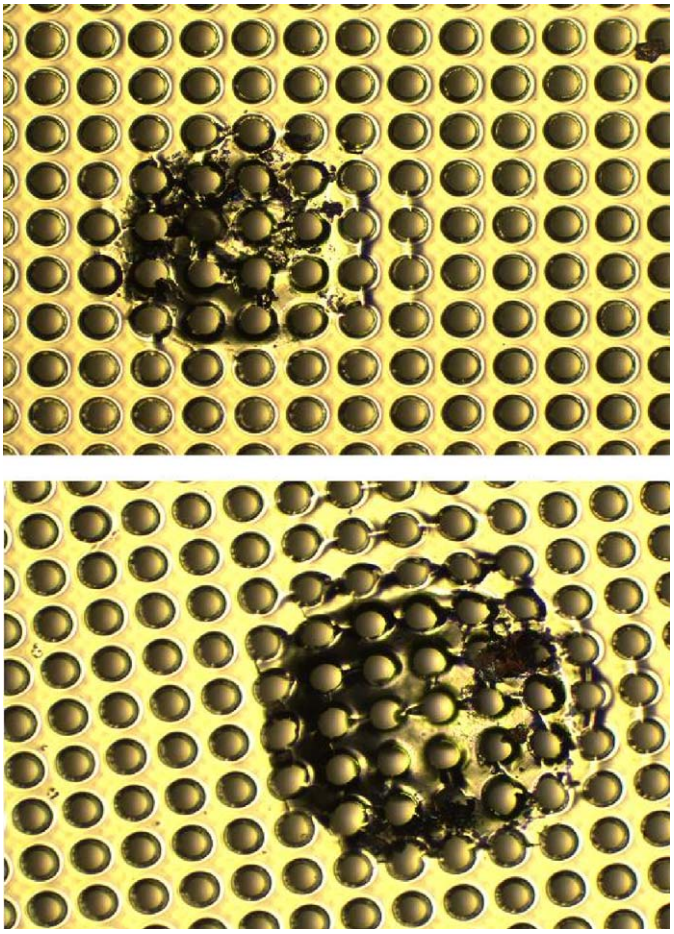

**Fig. 13.** Optical microscope image of a GEMGrid structure with recessed SU-8 after the drop test at 1 cm (top) and 5 cm (bottom).

Taking into account this effect the GEMGrid structure will be much less sensitive to humidity than InGrid devices.

Finally, InGrid and GEMGrid devices were exposed to air flow. The wind flow was generated from a compressed air gun with a 1.5 mm nozzle. The samples were placed at an angle of 45° with respect to the air flow. In both cases the metal grid peeled off from the SU-8 supporting structures but the SU-8 itself remained

attached to the substrate. On average, the wind speed needed to peel off the grid in the InGrid device was 80 km/h, while for the GEMGrid device the grid peeled off at 130 km/h. Such air flows are improbable in storage or detector operation conditions. However, dry-nitrogen blow cleaners, commonly applied during microsystem manufacturing and assembly, could operate in this regime. Hence, such instruments should be used carefully in the manufacturing of integrated grid structures, whether they are Micromegas like or GEM like.

## 6. Conclusions

A GEM-like structure was integrated on a Timepix chip to form a radiation imaging detector. It is fully functional and has a structural strength benefit compared to the integrated Micromegas (InGrid).

As with the InGrid approach, the microelectronic fabrication process introduces new geometrical design freedom in GEM-like detectors, offers pure materials and excellent dimensional control, and allows good alignment with the underlying patterned anode structure. It was found that the SU-8 dielectric should recess under the aluminum electrode to reach a sufficiently high-sparking limit.

Minimum ionizing particles and X-rays from an $^{55}$Fe source were detected. Three-dimensional tracking was feasible, and a single electron efficiency up to 82% was reached.

## Acknowledgements

This research is funded by the Dutch Foundation for Fundamental Research on Matter (FOM) and by the Dutch Technology Foundation STW through Project TET 6630 "Plenty of room at the top". The authors would like to thank Bijoy Rajasekharan, Joost Melai and Jiwu Lu for the cleanroom help, Sander M. Smits for mask design and J. Rövekamp for the mechanical support.

## References

[1] P. Colas, A.P. Colijn, A. Fornaini, Y. Giomataris, H. van der Graaf, E.H.M. Heijne, X. Llopart, J. Schmitz, J. Timmermans, J.L. Visschers, Nucl. Instr. and Meth. A 535 (1–2) (2004) 506.
[2] R. Bellazzini, F. Angelini, L. Baldini, F. Bitti, A. Brez, M. Ceccanti, L. Latronico, M.M. Massai, M. Minuti, N. Omodei, M. Razzano, C. Sgrò, G. Spandre, E. Costa, P. Soffitta, Nucl. Instr. and Meth. A 535 (1–2) (2004) 477.
[3] A. Bamberger, K. Desch, U. Renz, M. Titov, N. Vlasov, P. Wienemann, A. Zwerger, Nucl. Instr. and Meth. A 573 (3) (2007) 361.
[4] T. Kim, M. Freytsis, J. Button-Shafer, J. Kadyk, S.E. Vahsen, W.A. Wenzel, Nucl. Instr. and Meth. A 589 (2) (2008) 173.
[5] V.M. Blanco Carballo, M. Chefdeville, M. Fransen, H. van der Graaf, J. Melai, C. Salm, J. Schmitz, J. Timmermans, IEEE Electron Device Lett. 29 (6) (2008) 585.
[6] X. Llopart, R. Ballabriga, M. Campbell, L. Tlustos, W. Wong, Nucl. Instr. and Meth. A 581 (1–2) (2007) 485 Erratum, Nucl. Instr. and Meth. A. 585 (1–2) (2008) 106–108.
[7] X. Llopart, M. Campbell, R. Dinapoli, D. San Segundo, E. Pernigotti, IEEE Trans. Nucl. Sci. NS-49 (5) (2002) 2279.
[8] I. Giomataris, presentation at the micro-pattern gas detector (RD51) workshop, Amsterdam, 16–18 April 2008. http://indico.cern.ch/materialDisplay.py?contribId=15&sessionId=2&materialId=slides&confId=25069.
[9] J. Benlloch, A. Bressan, M. Capeáns, M. Gruwé, M. Hoch, J.C. Labbé, A. Placci, L. Ropelewski, F. Sauli, Nucl. Instr. and Meth. A 419 (2–3) (1998) 410.
[10] M. Bosma, V.M. Blanco Carballo, Y. Bylevich, M. Chefdeville, M. Fransen, H. van der Graaf, F. Hartjes, J. Melai, C. Salm, J. Schmitz, J. Timmermans, J.L. Visschers, N. Wyrsch, in: IEEE Nuclear Science Symposium Conference Record. NSS ′07, 6, 2007, 4631
[11] J. Kadyk, Nucl. Instr. and Meth. A 300 (3) (1991) 436.
[12] D. San Segundo Bello, M. van Beuzekom, P. Jansweijer, H. Verkooijen, J. Visschers, Nucl. Instr. and Meth. A 509 (1–3) (2003) 164.
[13] T. Holy, J. Jakubek, S. Pospisil, J. Uher, D. Vavrik, Z. Vykydal, Nucl. Instr. and Meth. A 563 (1) (2006) 254.
[14] M. Chefdeville, Development of Micromegas-like gaseous detectors using a pixel readout chip as collecting anode, Ph.D. Thesis, University of Amsterdam, 2009.
[15] S.T. Gulati, J.D. Helfinstine, J.F. Bayne, W.R. Powell, J.C. Lapp, Mechanical reliability of LCD panels under static loading, SID International Symposium Digest of Technical Papers 35(1) (2004) 1593, Paper 62.1.
[16] 〈http://www.intel.com/design/mobile/platform/downloads/fingerprintsensorproductguidelines.pdf〉.
[17] 〈http://www.veeco.com/〉.
[18] C. Salm, V.M. Blanco Carballo, J. Melai, J. Schmitz, Microelectron. Reliab. 48 (8–9) (2008) 1139.
[19] V.M. Blanco Carballo, J. Melai, C. Salm, J. Schmitz, Microelectron. Eng. 86 (4–6) (2009) 765.